# L-Phenylalanine Binding and Domain Organization in Human Phenylalanine Hydroxylase: A Differential Scanning Calorimetry Study†

Matthías Thórólfsson,‡ Beatriz Ibarra-Molero,§ Peter Fojan,|| Steffen B. Petersen,|| Jose M. Sanchez-Ruiz,*,§ and Aurora Martínez*,‡

*Department of Biochemistry and Molecular Biology, University of Bergen, Årstadveien 19, N-5009 Bergen, Norway, Departamento de Quimica Fisica, Facultad de Ciencias, 18071-Granada, Spain, and Department of Life Sciences, University of Aalborg, Sohngaardsholmsvej 49, DK-9000 Aalborg, Denmark*

*Received December 19, 2001; Revised Manuscript Received March 21, 2002*

ABSTRACT: Human phenylalanine hydroxylase (hPAH) is a tetrameric enzyme that catalyzes the hydroxylation of L-phenylalanine (L-Phe) to L-tyrosine; a dysfunction of this enzyme causes phenylketonuria. Each subunit in hPAH contains an N-terminal regulatory domain (Ser2−Ser110), a catalytic domain (Asp112−Arg410), and an oligomerization domain (Ser411−Lys452) including dimerization and tetramerization motifs. Two partially overlapping transitions are seen in differential scanning calorimetry (DSC) thermograms for wild-type hPAH in 0.1 M Na−Hepes buffer, 0.1 M NaCl, pH 7.0. Although these transitions are irreversible, studies on their scan-rate dependence support that the equilibrium thermodynamics analysis is permissible in this case. Comparison with the DSC thermograms for truncated forms of the enzyme, studies on the protein and L-Phe concentration effects on the transitions, and structure-energetic calculations based on a modeled structure support that the thermal denaturation of hPAH occurs in three stages: (i) unfolding of the four regulatory domains, which is responsible for the low-temperature calorimetric transition; (ii) unfolding of two (out of the four) catalytic domains, which is responsible for the high-temperature transition; and (iii) irreversible protein denaturation, which is likely responsible for the observed exothermic distortion in the high-temperature side of the high-temperature transition. Stages 1 and 2 do not appear to be two-state processes. We present an approach to the analysis of ligand effects on DSC transition temperatures, which is based on the general binding polynomial formalism and is not restricted to two-state transitions. Application of this approach to the L-Phe effect on the DSC thermograms for hPAH suggests that (i) there are no binding sites for L-Phe in the regulatory domains; therefore, contrary to the common belief, the activation of PAH by L-Phe seems to be the result of its homotropic cooperative binding to the active sites. (ii) The regulatory domain appears to be involved in cooperativity through its interactions with the catalytic and oligomerization domains; thus, upon regulatory domain unfolding, the cooperativity in the binding of L-Phe to the catalytic domains seems to be lost and the value of the L-Phe concentration corresponding to half-saturation is increased. Overall, our results contribute to the understanding of the conformational stability and the substrate-induced cooperative activation of this important enzyme.

Mammalian phenylalanine hydroxylase (phenylalanine 4-monooxygenase, PAH[1], EC 1.14.16.1) catalyzes the hydroxylation of L-phenylalanine (L-Phe) to L-tyrosine (L-Tyr), which is the initial and rate-limiting step in the catabolic pathway of L-Phe. Failure in the hydroxylation of L-Phe caused by mutations in the human PAH (hPAH) gene causes a serious disease in humans, phenylketonuria (PKU), one of the most prevalent disorders of amino acid metabolism. PAH belongs to the family of aromatic amino acid hydroxylases, which are non-heme iron containing- and tetrahydrobiopterin ($BH_4$)-dependent enzymes incorporating molecular oxygen into the ring of their substrates (*1*, *2*). The full-length wild-type hPAH (wt-hPAH) is a tetrameric protein of 451-residue subunits. As shown by deletion mutagenesis (*3*, *4*) and by the crystal structure (*5*−*7*), PAH has a three-domain structure. Each subunit contains (i) an N-terminal regulatory domain, up to Ser110, (ii) a catalytic domain (Asp111−Phe410), containing the active site iron and the substrate and $BH_4$ binding sites, and (iii) an oligomerization domain, with a dimerization motif (Ser411−Thr427) and a helical tetramerization motif at the C-terminus that promotes oligomerization through antiparallel helix−helix interactions (*6*).

† This work was supported by the Research Council of Norway, Meltzer L. Høyskolefond and Grant BIO2000-1437 from the Spanish Ministry of Science and Technology.

* To whom correspondence should be addressed. Fax: 34-958272879 (J.M.S.-R.), 47-55586400 (A.M.). E-mail: sanchezr@ugr.es (J.M.S.-R.), aurora.martinez@ibmb.uib.no (A.M.).

‡ University of Bergen.

§ Departamento de Quimica Fisica, Facultad de Ciencias.

|| University of Aalborg.

[1] Abbreviations: $BH_4$, (6*R*)-L-*erythro*-5,6,7,8-tetrahydrobiopterin; CD, circular dichroism; $C_p$, molar heat capacity; hPAH, human phenylalanine hydroxylase; wt-hPAH, wild-type hPAH; DLS, dynamic light scattering; DSC, differential scanning calorimetry; MBP, maltose binding protein; PAH, phenylalanine hydroxylase; PKU, phenylketonuria; wt-hPAH, wild-type full-length human phenylalanine hydroxylase.

10.1021/bi0160720 CCC: $22.00 
Published on Web 05/23/2002

PAH exhibits positive cooperativity for the binding of L-Phe as shown by steady-state kinetic measurements of the $BH_4$-dependent activity and by equilibrium binding analysis (for review see ref *8*). This sigmoidal dependence on L-Phe concentration seems to reflect a transition of the enzyme from a low-affinity and low-activity state to a high-affinity and high-activity state (*4*, *8*). The cooperativity of PAH in response to L-Phe concentration is believed to be of physiological significance as a mechanism controlling L-Phe homeostasis in blood, despite fluctuations in either dietary protein intake or protein turnover (*1*, *9*). Too rapid degradation of L-Phe will result in depletion of the stores of this essential amino acid, while its accumulation can lead to neurological damage, as seen in PKU. The cooperative activation of rat PAH by L-Phe has been interpreted to result from binding of the substrate either to (i) a putative allosteric/regulatory site, which is distinct from the catalytic site (*10*−*13*), or (ii) to the active site near the iron (*14*, *15*). However, the molecular basis of the cooperative response to L-Phe concentration is not known since the available crystal structures of PAH do not contain the full tetrameric structure and are only structures of truncated forms of the enzyme (*5*−*7*); in fact, we report in this work a tentative structural model of full-length hPAH prepared by combining the crystal structure of the regulatory and catalytic domains of rat PAH (*7*) with the crystal structure of the catalytic and oligomerization domains of hPAH (*6*). A similar topology for the composite model of PAH has also been obtained by others (*2*, *16*).

Equilibrium thermodynamics analysis of DSC thermograms for protein solutions can, in principle, provide a complete energetic description of the protein denaturation process [i.e., the number and energetic parameters of the significantly populated protein states (*17*)]. Furthermore, if this energetic description is interpreted in terms of suitable models, information regarding domain organization and interdomain interactions can be derived (*18*−*20*). We report here a differential scanning calorimetry study on the thermal denaturation of wt-hPAH and several truncated forms, addressed to gain insight into the relation between L-Phe binding and domain organization in hPAH. We will show that the two distinct transitions seen in the thermograms for wt-hPAH can be assigned to the denaturation of well-defined domains in the PAH structure. Although these two transitions are irreversible, analysis of the scan-rate dependence of the thermograms will support the applicability of the equilibrium thermodynamics analysis in this case.

## EXPERIMENTAL PROCEDURES

*Preparation of hPAH Forms*. Expression of recombinant wt-hPAH (*21*), its active truncated forms hPAH(Asp112−Lys452) and hPAH(Ser2−Gln428) (*4*) and the N-terminal regulatory domain (*22*) in *Escherichia coli* (TB1) as fusion protein with maltose-binding protein (MBP), purification of the fusion proteins by affinity chromatography on amylose resin (New England Biolabs), cleavage by factor Xa (New England Biolabs), and further purification by high-performance size exclusion chromatography on a HiLoad Superdex column (1.6 × 60 cm) were performed as described (*4*, *21*). Protein concentration of the purified hPAH forms was determined by the absorbance at 280 nm, using the absorption coefficient $A_{280}$ (for 1 mg $mL^{-1}$ $cm^{-1}$) = 1.0 (*21*).

*Differential Scanning Calorimetry (DSC).* Measurements were performed on a MicroCal VP-DSC differential scanning calorimeter (MicroCal Inc.) with cell volumes of 0.5 mL at the indicated scan rates. A 0.1 M Na−Hepes buffer, 0.1 M NaCl, pH 7.0 was used in all experiments. Calorimetric cells were kept under an excess pressure of 30 psi to prevent degassing during the scan. Purified tetramers of wt-hPAH and hPAH(Asp112−Lys452), purified dimers of hPAH-(Ser2−Gln428), and cleaved purified fusion protein of the N-terminal domain (hPAH(Ser2−Ser110)) were used. Protein concentrations were about 30 $\mu$M per subunit hPAH in all experiments, except as otherwise indicated. Equimolar amounts of ferrous ammonium sulfate per enzyme subunit were added to convert some iron-free apoenzyme present in the samples into holoenzyme (*22*). Further details about the calorimetric experiments and the calorimetric data processing can be found elsewhere (*23*). Fittings of theoretical equations to the experimental heat capacity profiles and the experimental L-Phe effect on transition temperatures were carried out using a program written by us in the MLAB environment (Civilized Software, Inc.). Accessible surface areas used in the theoretical predictions of energetic parameters were calculated using the Shrake-Rupley algorithm (*24*) with a radius of 1.4 Å for the solvent probe and the Chothia set for the protein atoms (*25*).

*Circular Dichroism (CD).* CD measurements were performed on a Jasco J-810 spectropolarimeter equipped with a Jasco 423S Peltier element for temperature control. Enzyme samples were prepared in 15 mM sodium phosphate, 0.15 M NaCl, pH 7.0, and placed in quartz cells with a path length of 1 mm. Protein thermal denaturation was monitored by following the changes in ellipticity at 222 nm, with a scan rate of 0.7 K/min and with a protein concentration of 25 $\mu$M per subunit. Spectra were recorded in the temperature range 25−70 °C. Analysis of the data and determination of midpoint melting temperature ($T_m$) values were performed by noise reduction and differentiation of the curves using the Standard Analysis program provided with the instrument.

*Dynamic Light Scattering (DLS).* DLS was performed using a DynaPro-MSTC Temperature-Controlled DLS instrument (Protein Solutions Inc.). DLS data were analyzed by the autocorrelation method to measure the hydrodynamic radius and the polydispersity (*26*) of solutions of wt-hPAH (60 $\mu$L, 30 $\mu$M subunit). The results were analyzed applying monomodal and bimodal models (*27*).

*Molecular Modeling.* A complete structural model for wt-hPAH including the tetramerization motif was generated by aligning the catalytic domains of the dimeric form of rat PAH (Ser2−Gln429) (PDB accession code 2PHM) and the tetrameric N-terminal truncated hPAH(Val118−Lys452) (PDB accession code 2PAH) using the programs Swiss-PdbViewer (GlaxoSmithKline R&D), InsightII (Accelrys), and Midas Plus (U. C. San Francisco) (*28*). Figures were generated using the program WebLab ViewerPro (Accelrys).

## RESULTS AND DISCUSSION

*Wild-Type-PAH and Its Truncated Forms.* We have recently described the expression and the kinetic and molecular characterization of recombinant wt-hPAH and of truncated forms of the enzyme (*4*, *21*, *22*). The catalytic and physicochemical properties of the full-length enzyme are

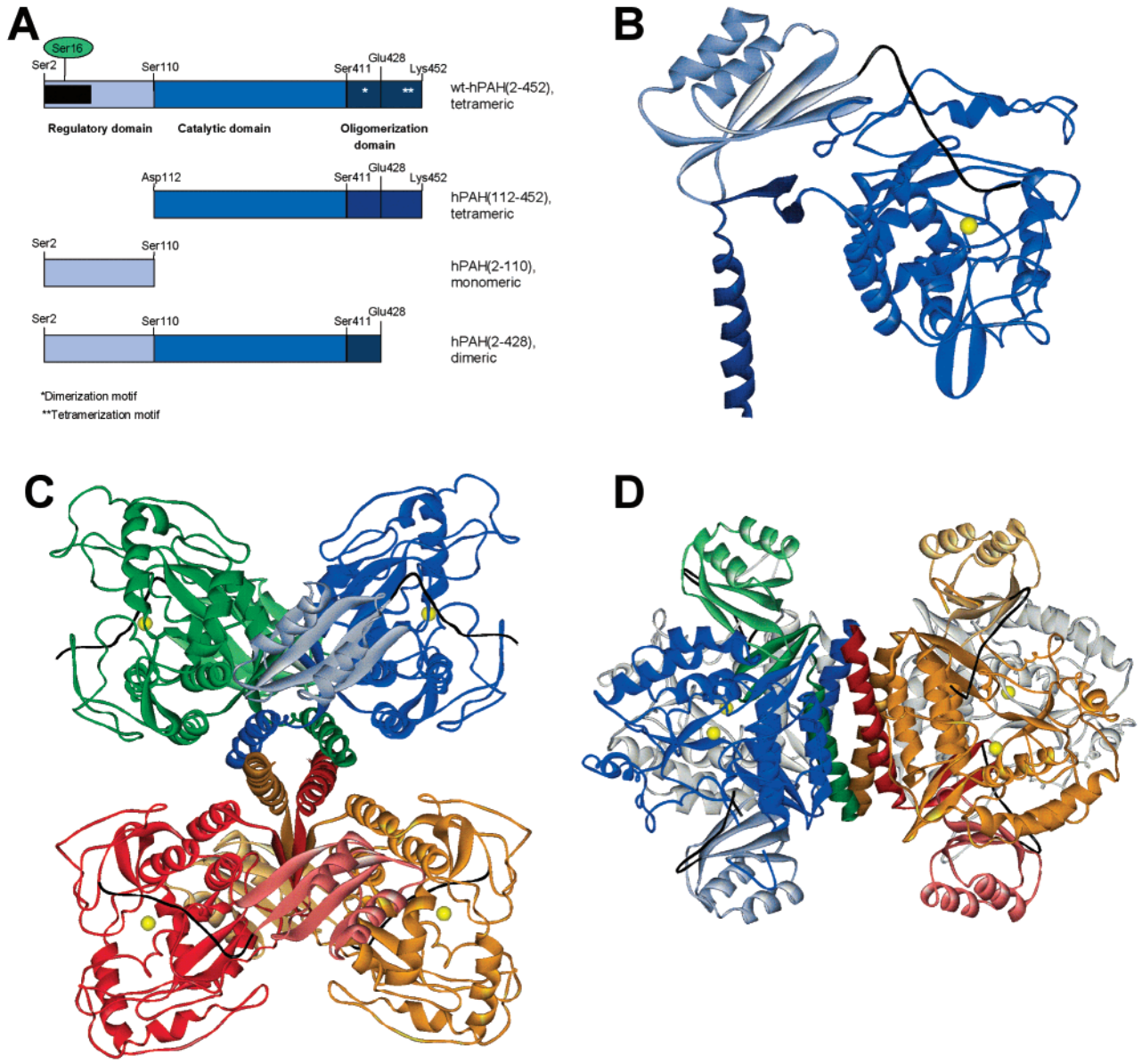


FIGURE 1: The domain structure of human phenylalanine hydroxylase (hPAH). (A) Schematic representation of the different hPAH forms used in this work, illustrating their functional domains. The structure of monomeric (B) and tetrameric (C and D) full-length hPAH was modeled using as templates the crystal structures of both truncated dimeric rat PAH (2−428) (PDB 2PHM) (*7*) and tetrameric hPAH (111−452) (PDB 2PAH) (*6*). The catalytic Fe is shown in yellow and the N-terminal autoegulatory sequence (up to Gly33) is in black. In panel D, the catalytic domains of the subunits at the backside of the figure are depicted in light gray for clarity.

essentially the same as reported for PAH isolated from human liver (*21*, *29*). The hPAH forms used in this work were (i) tetrameric full-length wt-hPAH(Ser2−Lys452), including the three domains in the enzyme, (ii) tetrameric hPAH(Asp112−Lys452), including the catalytic and oligomerization domains, (iii) the N-terminal regulatory domain hPAH(Ser2−Ser110), which was devoid of catalytic activity, and (iv) the dimeric hPAH(Ser2−Glu428), including the regulatory domain, the catalytic domain, and the dimerization motif. In addition, truncated forms lacking the dimerization motif, i.e., hPAH(Ser2−Arg400), were created to prepare monomeric forms of the enzyme. However, the expression of these deletion mutants resulted only in aggregated and precipitated protein (*4*). In Figure 1 is shown a schematic representation of the hPAH forms used in this study and a structural model of full-length tetrameric hPAH created using as templates the crystal structures of both truncated dimeric rat PAH (2−428) (*7*) and tetrameric hPAH (111−452) (*6*). As seen in the modeled structure of hPAH, in each subunit the oligomerization domain establishes contacts with both the N-terminal domain and the catalytic domain (Figure 1B). Moreover, the regulatory domain from one subunit is composed both of an α−*β* sandwich (*β*α*ββ*α*β*) core, which establishes contacts with the catalytic domain of the other subunit in the dimer through the loop Arg68−Asp75, and of an extended N-terminal autoregulatory sequence, which covers the active site of the corresponding subunit (Figure 1C,D). The subunits reorganize in the tetramer as a dimer of dimers and the subunits in one dimer contact the subunits in the adjacent dimer only via the α-helical tetramerization motif (Figure 1C,D).

*Assessment of the Low-Temperature Oligomeric State of the hPAH Forms Used in this Work.* The oligomeric state at pH 7.0 and low-temperature of the full-length and truncated

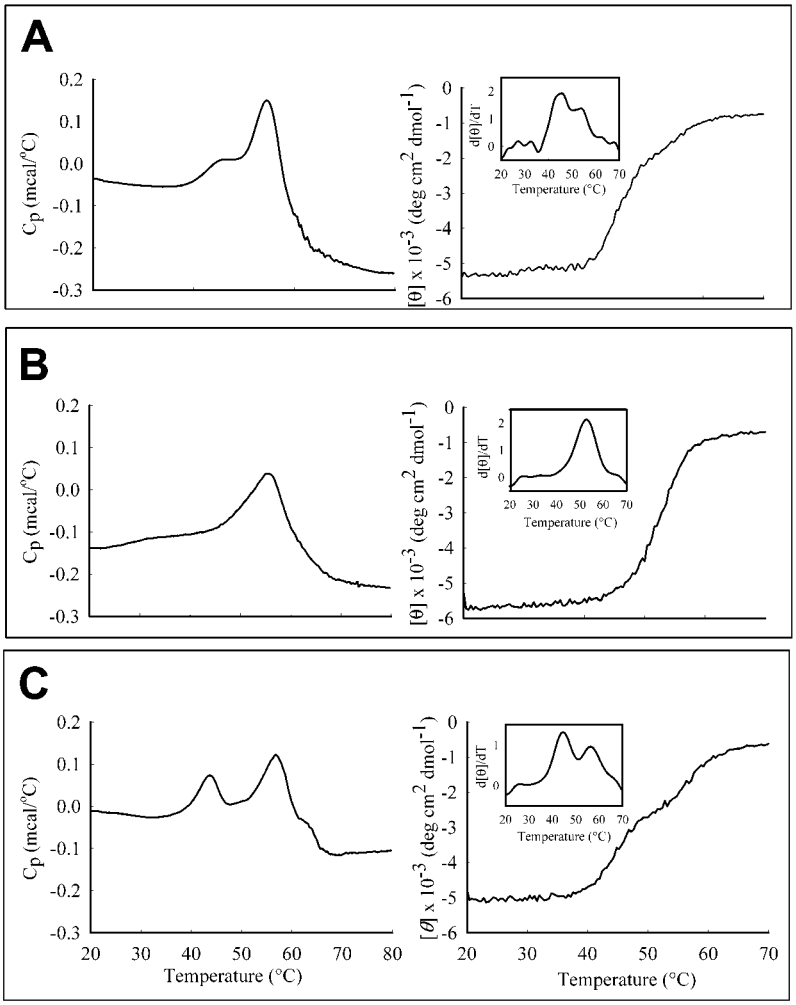


FIGURE 2: DSC- (left) and CD- (right) monitored thermal denaturation of full-length wt-hPAH and its truncated forms. Samples (30 $\mu$M subunit): wt-hPAH (A), hPAH(Asp112-Lys452) (B), and hPAH(Ser2-Glu428) (C). The DSC thermograms were acquired in 0.1 M Na−Hepes, 0.1 M NaCl, pH 7.0, at a scan rate of 0.7 K/min, while for the CD-monitored thermal scans the changes in ellipticity at 222 nm are acquired for samples prepared in 15 mM sodium phosphate, 0.15 M NaCl, pH 7.0, at a scan rate of 0.7 K/min. Original DSC traces after baseline subtraction are shown. Inset: first derivatives of the CD-monitored temperature scans.

forms of hPAH used in this work was determined by high-resolution size-exclusion chromatography (*4*). We found that, within the 4−20 °C temperature range and the 0.1−50 mg/mL protein concentration range, wt-hPAH and hPAH-(Asp112−Lys452) were tetrameric, while hPAH(Ser2−Glu428) was dimeric. The oligomeric state of wt-hPAH was also studied by DLS. The observed hydrodynamic radius for the wt-hPAH at 20 °C, calculated using a monomodal model, was 57.7 ± 0.2 Å, in agreement with a distance of 117 Å between the two most distant atoms in the model of the tetramer (Figure 1). In the presence of 1−5 mM L-Phe, the estimated radius was 60.0 ± 0.1 Å, slightly larger than that of the nonactivated enzyme, but still consistent with the tetrameric character of wt-PAH. High resolution size-exclusion chromatography studies have also shown only a slight increase of the Stokes radius of the tetrameric wt-hPAH in the presence of L-Phe (*30*).

*General Description of the DSC Thermograms for the Thermal Denaturation of PAH*. Preliminary calorimetric studies at pH 5.5, 7.0, and 8.5 indicated highest thermal stability at pH 7.0 for both wt-hPAH and hPAH(Asp112−Lys452), and further studies were performed at this pH value. Figure 2 shows an illustrative example of the DSC thermograms for the thermal denaturation of the several forms of PAH studied in this work. Several points must be noted:

(i) Two partially overlapping transitions (centered at about 46 and 54 °C) are apparent in the thermogram for tetrameric wt-hPAH (Figure 2A). This result is confirmed by the corresponding CD denaturation profile that shows two distinct sigmoidal transitions with midpoints temperatures close to the temperatures of the maxima of the DSC transitions (Figure 2A).

(ii) Only the high-temperature transition is observed in the thermograms for a truncated PAH form that lacks the regulatory domain, as well as in the corresponding CD denaturation profile (Figure 2B). This result strongly suggests that the low-temperature transition is due to the denaturation of the regulatory domain and that the denaturation of catalytic domains is involved in the high-temperature transition. This assignment will be confirmed and refined by the analysis of the effect of L-Phe on the DSC thermograms given further below.

(iii) No information regarding the interactions between the folded regulatory and catalytic domains can be derived from the comparison between the denaturation profiles shown in Figure 2A,B. Note that, according to the interpretation given

above, the denaturation of the catalytic domains in tetrameric wt-hPAH occurs essentially after the regulatory domains have denatured and, in the case of hPAH(112−452), the regulatory domain is absent. Therefore, from the similarity of the transition temperatures for the catalytic domain in wt-hPAH and hPAH(112−452) (Figure 2A,B), we can only infer that there appears to be little interaction between the folded catalytic domain and the *denatured* regulatory domain.[2]

(iv) Some qualitative insight into intramolecular interactions in hPAH can be derived, however, from the comparison with the denaturation profiles for other truncated forms. Thus, the truncated form corresponding to the regulatory N-terminal domain hPAH(Ser2−Ser110) did not show a transition, in agreement with our earlier thermostability studies by IR spectroscopy (*22*); this result suggests that hPAH(Ser2−Ser110) is not correctly folded and, thus, that interactions with the rest of the molecule are necessary for the correct folding of the regulatory domain. On the other hand, two transitions are observed in the thermogram and CD denaturation profile (Figure 2C) for hPAH(2−428), the truncated form that lacks the tetramerization motif; actually, the transition temperatures for this dimeric form are similar to those found for the tetrameric hPAH.

(v) The thermal denaturation of wt-hPAH and the several truncated forms was always irreversible (in the absence and presence of L-Phe), as no transition could be detected in reheating runs (not even when the first run had been stopped immediately after the end of the second transition). Aggregation was evident in the samples extracted from the calorimetric cells. After the standard baseline corrections, the DSC thermograms for wt-hPAH and the truncated forms often seemed to suggest a negative value for the denaturation heat capacity change (see Figure 2). We attribute this physically unrealistic result to a distortion of the high-temperature transition due to aggregation.

*The Scan Rate Effect on the DSC Thermograms for the Thermal Denaturation of PAH.* Analysis of DSC thermograms for protein solutions according to equilibrium thermodynamics can provide a complete description of the temperature-induced denaturation process in terms of the number and energetic features of the significantly populated states (*17*). This analysis is, however, seriously hampered in cases of irreversible denaturation, since irreversible alterations of proteins are kinetic processes, which cannot be described by equilibrium thermodynamics (*31*). In fact, in many cases of irreversible denaturation, the DSC thermograms have been found to conform to a two-state kinetic model (see ref *32* and references quoted therein), which implies that no information about the equilibrium denaturation process is available. On the other hand, in a few cases, the analysis of the scan-rate effect on the DSC transitions has supported the equilibrium thermodynamics analysis of irreversible DSC termograms (see, for instance, ref *33*). Thus, theoretical simulations based on Lumry-Eyring models (*31*, *34*) indicate that (i) kinetic distortions of DSC transitions are reflected in a scan-rate dependency of the transitions; (ii) kinetic distortions due to irreversible processes must become negligible at sufficiently high scan-rates (strictly, in the scan-rate $\rightarrow \infty$ limit). The scan-rate range of commercial DSC instruments is rather limited and, very often, the distortions caused by irreversibility are not eliminated, not even at the highest scan-rate available. However, in the case of annexin V E17G, Hinz and co-workers (*33*) found that the plot of transition temperature versus scan-rate for the 0.1−2.5 K/min range showed clear signs of reaching a plateau, a result that supported the applicability of the equilibrium thermodynamics analysis to the DSC thermograms obtained at the highest scan-rate employed. We show in Figure 3 the same type of plots for the two transitions seen in the thermograms for hPAH denaturation; note that we include in Figure 3 data obtained in the absence of L-Phe and in the presence of a representative concentration of this ligand. The plots of Figure 3 are qualitatively similar to that reported by Vogl et al. for annexin, although, in our case, the plateaus are more clearly defined; thus, there appears to be little or no scan-rate effect on the transition temperatures within the 0.6−1.3 K/min range, which supports that, for those scan-rates, kinetic distortions become negligible and the equilibrium thermodynamics analysis is feasible, at least up to about the transition temperature for the high-temperature transition (whose high-temperature side is likely distorted by aggregation, as we have previously noted).

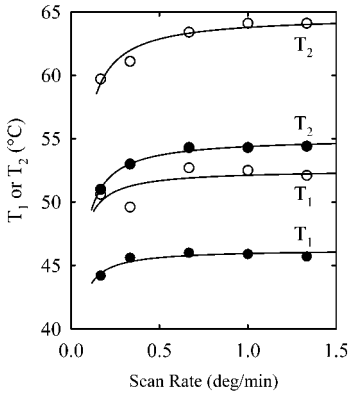


FIGURE 3: Scan-rate effect on the transition temperatures for the two transitions observed in the DSC thermograms for the thermal denaturation of wt-hPAH. Closed symbols, transition temperatures in the absence of L-Phe. Open symbols, transition temperatures in the presence of 22 mM L-Phe. The continuous lines have no theoretical meaning and are shown to guide the eye.

*The Effect of Protein Concentration on the DSC Thermograms for the Thermal Denaturation of wt-hPAH.* Under the conditions employed in this work, wt-hPAH is a tetramer at room temperature (see the previous section: "Assessment

[2] In principle, information regarding interdomain interactions in a two-domain protein (A−B) can be obtained if the *two* partially folded states ($A_{folded} - B_{unfolded}$ and $A_{unfolded} - B_{folded}$) become significantly populated during the thermally induced denaturation and the energetic parameters *for both of them* can be determined from the analysis of the experimental DSC profiles and combined with those for the native state ($A_{folded} - B_{folded}$), to yield the unfolding changes in energetic parameters for each domain when the other domain is folded and when the other domain is unfolded (*18*−*20*). In the case of wt-hPAH, the studies reported in this work indicate that the regulatory domains are less stable than the catalytic domains and denature at significantly lower temperatures. Thus, the population of the partially folded state in which regulatory domains are folded and catalytic domains are unfolded is expected to be rather low during the scan, and it appears highly unlikely that its energetic parameters could be determined from the analysis of the experimental DSC for wt-hPAH (in particular, since the distortion of the high-temperature transition due probably to aggregation makes the chemical baseline uncertain). Therefore, we have *not* attempted to obtain information about interdomain interactions in wt-hPAH from the fitting of theoretical models to the experimental thermograms and interdomain interactions are not, in fact, included in our fitting equation (eq 1).

of the Low-Temperature Oligomeric State of the hPAH Forms Used in this Work"); therefore, we could expect its temperature-induced denaturation to be accompanied by dissociation, which will necessarily imply that the DSC thermograms would depend on total protein concentration (*31*, *35*, *36*). However, no significant effect was detected within a wide protein concentration range (7.5−90.0 $\mu$M per subunit) (results not shown). This result strongly suggests that denaturation processes responsible for the two transitions seen in the DSC thermograms for wt-hPAH do not involve subunit dissociation. It appears, therefore, that wt-hPAH remains tetrameric during most of the denaturation temperature range, which suggests a high stability for the oligomerization domain. It is also possible that the denaturation of the tetramerization and dimerization motifs occurs, with little thermal effect and with concomitant dissociation and aggregation, in the high-temperature side of the high-temperature transition. In any case, the immediate consequence of the lack of experimental protein concentration effect is that the fitting of the DSC thermograms can be carried out using models that do not include changes in oligomerization state (next section).

*Fitting of the DSC Thermograms for the Thermal Denaturation of wt-hPAH.* Fitting of the DSC thermograms for the thermal denaturation of wt-hPAH in the absence of L-Phe and in the presence of several concentrations of this ligand (within the range 30 $\mu$M−25 mM) was carried out using the following equation:[2]

$$C_p = C_{P,N} + \frac{\Delta H_1 \Delta H_1^{VH}}{RT^2} \frac{K_1}{(1+K_1)^2} + \frac{\Delta H_2 \Delta H_2^{VH}}{RT^2} \frac{K_2}{(1+K_2)^2} \quad (1)$$

where the native (N) (low-temperature) baseline is assumed linear in temperature [$C_{P,N} = a + bT$] and the equilibrium constants are given by

$$K_i = \exp\left[-\frac{\Delta H_i^{VH}}{R}\left(\frac{1}{T} - \frac{1}{T_i}\right)\right] \quad (2)$$

with *i* equal to 1 or 2. Several features of the fitting process must be noted: (i) Equation 1 includes terms corresponding to two non-two-state transitions described phenomenologically in terms of van't Hoff enthalpy values ($\Delta H_i^{VH}$), which may differ from the corresponding calorimetric enthalpies ($\Delta H_i$). (ii) Since the high-temperature side of the high-temperature transition is very likely distorted by aggregation, we have only fitted a limited temperature range, ending a few degrees above the temperature of the maximum heat capacity for the high-temperature transition. (iii) It is clear that the experimental data used in the fitting process do not contain information about denaturation heat capacity changes that, accordingly, are not included in eq 1.

Fittings to the thermograms obtained in the absence and presence of several L-Phe concentrations were always excellent (see Figure 4 for representative examples), and the calorimeric and van't Hoff enthalpy values determined from the fitting did not depend significantly on ligand concentration or temperature, within the scatter of the determined values. The average values and standard deviation for the determined enthalpy values are given in Table 1 and the determined transition temperatures are given in Figure 5.

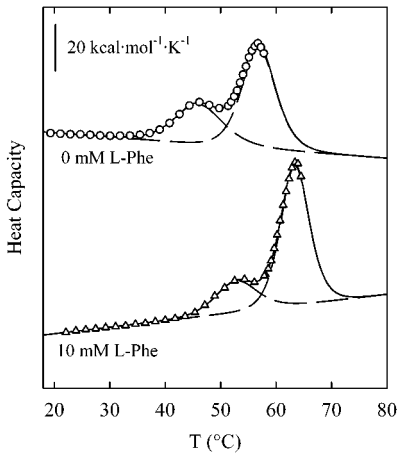


FIGURE 4: Heat capacity versus temperature profiles for the thermal denaturation of wt-hPAH in the absence of L-Phe and in the presence of 10 mM L-Phe. (○,△), experimental heat capacity data. The continuous lines represent the best fits of the sum of two non-two-state transitions (eq 1) to the experimental data; the individual transitions resulting from the fitting are shown with dashed lines. Note that the profiles have been displaced in the *y*-axis for the sake of clarity.

Table 1: Average Values of the Calorimetric Enthalpy ($\Delta H_i$), Van't Hoff Enthalpy ($\Delta H_i^{VH}$) and Calorimetric to Van't Hoff Enthalpy Ratio (*r*) Derived from the Analysis of DSC Thermograms for the Thermal Denaturation of wt-hPAH in the Absence of L-Phe and in the Presence of Several Concentrations of L-Phe

| | $\Delta H_i$, kcal (mol of tetramer)$^{-1}$ | $\Delta H_i^{VH}$, kcal/mol | *r* |
|---|---|---|---|
| transition 1 (low-T) | 160 ± 44 | 87 ± 18 | 1.83 ± 0.67 |
| transition 2 (high-T) | 324 ± 28 | 124 ± 14 | 2.63 ± 0.31 |

Note that since the temperature dependence of the enthalpy values is not detected within the experimental scatter, the average values given in Table 1 are to be assigned to the average values of the $T_1$ and $T_2$ transition temperatures determined for the whole range of L-Phe concentrations (50 °C for the low-T transition and 59 °C for the high-T transition). Note also that the calorimetric enthalpy values are given per mole of tetramer and that the calorimetric to van't Hoff enthalpy ratios for both transitions are close to 2.

*Unfolding Enthalpy Values from Structure-Energetics Relationships.* We have also calculated theoretical enthalpy change values on the basis of our modeled structure (Figure 1) and the structure-energetics relationships developed by Freire and co-workers (*37*, *38*); thus, the heat capacity change and the enthalpy change at 60 °C can be related to changes in apolar and polar accessible surface area through

$$\Delta C_p = 0.45\Delta ASA_{ap} - 0.26\Delta ASA_{pol} \quad (3)$$

$$\Delta H_{60} = -8.44\Delta ASA_{ap} + 31.4\Delta ASA_{pol} \quad (4)$$

where the changes in accessible surface area are in Å$^2$, $\Delta C_P$ is in cal K$^{-1}$ mol$^{-1}$, and $\Delta H_{60}$ is cal/mol. Although eq 4 gives $\Delta H$ at the reference temperature of 60 °C, $\Delta H$ at other temperature can be calculated from $\Delta H_{60}$ and $\Delta C_p$ (eq 3) using the Kirchoff equation.

We show in Table 2 the changes in accessible surface area calculated for the unfolding of the four regulatory domains and the unfolding of the four catalytic domains (with the

Table 2: Unfolding Changes in Apolar and Polar Accessible Surface Area ($\Delta ASA_{Ap}$ and $\Delta ASA_{pol}$) and Theoretical Values for Unfolding Heat Capacity ($\Delta C_p$) and Enthalpy Changes at 60 °C ($\Delta H_{60}$) and at the Given Temperatures ($\Delta H$) Derived from the Modeled wt-hPAH Structure Using Structure-Energetics Correlations

| unfolding of | $\Delta ASA_{ap}$ (Å$^2$) | $\Delta ASA_{pol}$ (Å$^2$) | $\Delta C_p$ (kcal K$^{-1}$ mol$^{-1}$) | $\Delta H_{60}$ (kcal/mol) | $\Delta H$ (kcal/mol) |
|---|---|---|---|---|---|
| four regulatory domains | 24235 | 14973 | 7.0 | 266[a] | 196[a] (at 50 °C) |
| | | | | 234[b] | 164[b] (at 50 °C) |
| four catalytic domains | 73358 | 41231 | 22.3 | 676[a] | 654[a] (at 59 °C) |
| | | | | 589[b] | 567[b] (at 59 °C) |

[a] Values calculated on the basis of eq 4. [b] Values calculated on the basis of eq 6.

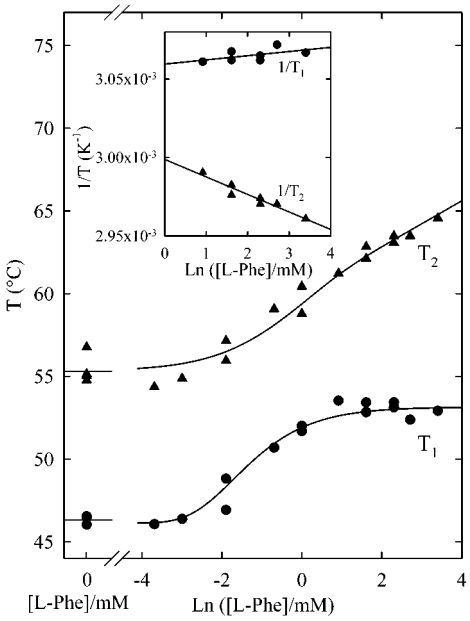


FIGURE 5: Effect of L-Phe concentration on the transition temperatures for the two transitions observed in the DSC thermograms for the thermal denaturation of wt-hPAH. The symbols are the values of $T_1$ and $T_2$ derived from the experimental thermograms, and the continuous lines represent the best fit of the dependencies given by eqs 25−29 to the experimental values. Inset: plots of $1/T_1$ and $1/T_2$ versus logarithm of L-Phe concentration (see eq 17).

regulatory domains already unfolded); this calculation used our modeled structure (Figure 1) for the folded regions of the protein and an extended chain as a model for the unfolded regions. The $\Delta C_p$ and $\Delta H_{60}$ values derived from these $\Delta ASA$ values using eqs 3 and 4 are also given in Table 2. Finally, we have calculated (Table 2), from these $\Delta C_p$ and $\Delta H_{60}$ values, $\Delta H$ for the unfolding of the regulatory domains at 50 °C (the average of our experimental $T_1$ values) and $\Delta H$ for the unfolding of the four catalytic domains at 59 °C (the average of our experimental $T_2$ values), so that a comparison with the experimental $\Delta H$ values can be made. This comparison leads to a surprising outcome: the calculated enthalpy change (Table 2) for the unfolding of the four regulatory domains (196 kcal/mol) is in good agreement with the experimental unfolding enthalpy change for the low-temperature transition (160 ± 44 kcal/mol); however, the calculated enthalpy change for the unfolding of the catalytic domains (654 kcal/mol) is twice the experimental value for the high-temperature transition (324 ± 28 kcal/mol)! This suggests that only two catalytic domains (out of the four in the tetramer) actually unfold in the high-temperature transition (or, at least, in the part of the high-temperature transition amenable to equilibrium thermodynamics analysis). This suggestion may appear at first so surprising that it seems convenient to discuss this enthalpy discrepancy in some detail, as well as the molecular reasons for the possible differences in stability between the different catalytic domains. In particular, the following five points must be noted:

(i) We cannot attribute the enthalpy discrepancy to fitting uncertainties associated with the need for truncating the experimental heat capacity data at about the $T_m$ of the second transition (Figure 4). Thus, we compare in Figure 6 a representative DSC profile for wt-hPAH with the theoretical profiles calculated using for the high-T transition the $\Delta H$ value of 654 kcal/mol derived from the structure-energetics relationships, together with different values of the van't Hoff enthalpy (see legend to Figure 6 for further details on the calculation of the theoretical profiles). The calculated profiles corresponding to calorimetric to van't Hoff enthalpy ratios ($r$) of 4, 2, and 1 show a very large high-temperature transition, in clear disagreement with the experimental thermogram (Figure 6A). Values of $r$ higher than 4 yield very broad high-temperature transitions that are not well resolved from the low-temperature one, in disagreement again with the experimental profiles (Figure 6B). We conclude that the experimental profiles are not consistent with a $\Delta H$ of about 600 kcal/mol for the high-temperature transition.

(ii) We cannot attribute the enthalpy discrepancy to a packing density for the catalytic domains significantly different than the average packing density of the proteins analyzed to obtain eq 4. Thus, following Freire and coworkers (*37*), we have calculated, for different types of atom pairs ($x-y$) in the catalytic domains of wt-hPAH, the energy weighted distance average defined as

$$\langle R_{x-y}, w\rangle = \sum R_{i,j}(E_{i,j}/E_{TOT}) \qquad (5)$$

where $R_{i,j}$ is the separation between atoms $i$ and $j$, $E_{i,j}$ is the energy of that pair calculated from the Lennard-Jones equation with the parameters of Levitt (*39*), and $E_{TOT}$ is the total energy for all the $x-y$ atom pairs. The average of the values obtained for the four catalytic domains were 5.73 ± 0.01 (C−C), 5.27 ± 0.01 (C−O), 5.70 ± 0.01 (CO−C), 4.27 ± 0.01 (CO−N), 4.92 ± 0.01 (CO−O), 4.057 ± 0.001 (O−N), and 6.16 ± 0.02 (O−O), where the types of atom pairs have been indicated in parentheses (CO stands for the carboxyl carbon). Most of these values are slightly larger (and, hence, indicate a slightly less dense packing) than those for the set of 15 proteins analyzed in ref *37*): 5.54 ± 0.07 (C−C), 5.07 ± 0.08 (C−O), 5.58 ± 0.13 (CO−C), 4.39 ± 0.16 (CO−N), 4.68 ± 0.08 (CO−O), 3.92 ± 0.10 (O−N), and 5.89 ± 0.08 (O−O). We have also calculated the dimensionless packing parameters for the apolar−apolar, polar−polar, and apolar−polar interactions ($U_{ap}$, $U_{pol}$, $U_{mix}$) as defined in ref *37*: $U_{ap} = 0.698$, $U_{pol} = 0.718$, $U_{mix} = 0.704$ for the regulatory domains, and $U_{ap} = 0.697$, $U_{pol} =$

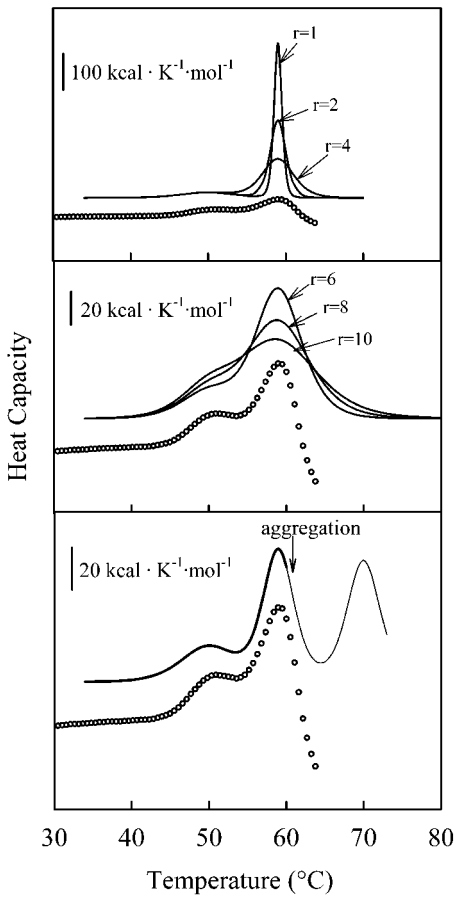


FIGURE 6: Comparison between theoretical and experimental heat capacity profiles for wt-hPAH. Note that the profiles have been displaced in the *y*-axis for the sake of clarity. The experimental profile (the same in the three panels and shown with open circles) was obtained with a L-Phe concentration of 0.5 mM. Theoretical profiles (shown with continuous lines) were calculated as sums of non-two-state transitions (eq 1). The lower temperature transition (corresponding to the unfolding of the regulatory domains) was simulated using as $\Delta H_1$, $T_1$, and calorimetric to van't Hoff enthalpy ratio, the average values derived from the analysis of the experimental thermograms ($\Delta H_1 = 160$ kcal/mol, $T_1 = 50$ °C, and $r = 1.83$). The high-temperature transitions in (A) and (B) were simulated using the average $T_2$ value from the experimental profiles (59 °C), a $\Delta H_2$ value for the unfolding of the 4 catalytic domain calculated from structure-energetics correlations (654 kcal/mol) and different values for the calorimetric to van't Hoff enthalpy ratio (shown alongside the profiles). Note that theoretical excess heat capacity profiles are displayed; inclusion of the chemical baseline would mainly "raise" the high-temperature transition, making even more evident the discrepancy between experimental and calculated profiles. (C) This panel illustrates a likely scenario for the thermal denaturation of wt-hPAH: two catalytic domains (simulated with $\Delta H = 327$ kcal/mol) unfold with a transition temperature of 59 °C, while the two remaining catalytic domains show higher stability; their unfolding transition (see thinner line in the simulated equilibrium unfolding profile) is not seen in the experimental profile (open circles) because protein aggregation occurs a few degrees above 59 °C.

0.719, $U_{mix} = 0.703$ for the catalytic domains. These values allow us to calculate unfolding enthalpy values using an extension of eq 4 that considers explicitly the effect of packing (eq 14 in ref *37*):

$$\Delta H_{60} = (\alpha_{ap} + \beta_{ap}U_{ap}{}^6)\Delta ASA_{ap} + (\alpha_{pol} + \beta_{pol}U_{pol}{}^6)\Delta ASA_{pol} + \beta_{mix}U_{mix}{}^6\Delta ASA_{total} \quad (6)$$

where $\alpha_{ap} = -12.46$, $\beta_{ap} = 25.34$, $\alpha_{pol} = 24.38$, $\beta_{pol} = 16.57$, and $\beta_{mix} = 16.42$ for $\Delta H_{60}$ in cal/mol and ASA values in Å$^2$. The $\Delta H$ values obtained using eq 6 (see Table 2) are somewhat lower than those derived from eq 4, but, still, the experimental $\Delta H$ value for the high-temperature transition is about half the value predicted for the unfolding of the four catalytic domains.

(iii) We cannot attribute the enthalpy discrepancy to enthalpy effects associated with changes in the protonation state of His side-chains (other ionizable side-chains rarely have p*K* values in the vicinity of 7). Normal p*K* values for His are around 6.3−6.8, although perturbed values may be found, particularly in native states. The ionization enthalpy for His is about 7 kcal/mol (*40*), and there are nine His residues in each catalytic domain. Therefore, a total ionization contribution to $\Delta H$ comparable to the enthalpy discrepancy could only be obtained by assuming the extremely unlikely scenario that all or almost all the 36 His side-chains in the four catalytic domains have strongly perturbed p*K* values, in such a way that they completely change their protonation state upon unfolding (note also that this would imply that about 36 protons are involved in the unfolding process with the concomitant very strong pH effect on transition temperatures, an effect which is not observed experimentally).

(iv) Differences in stability between the different catalytic domains may be in fact expected from the structure of wt-hPAH. Thus, the X-ray structure of a tetrameric truncated form of wt-hPAH comprising the catalytic and oligomerization domains was found to be clearly asymmetric and show two conformationally different "dimers" (*6*). The distortion of the tetrameric symmetry was evident from the reported surface calculations, which indicated differences of about 500 Å$^2$ between the different dimerization interfaces (see ref *6* for further details); such a difference is expected to have a significant energetic impact. Therefore, a likely scenario for wt-hPAH unfolding is that two (out of the four) catalytic domains have a denaturation temperature higher than 60 °C, but that their unfolding (and that of the oligomerization domains) is not observed in the experimental DSC thermograms because aggregation occurs before the corresponding temperature range is reached. An illustration of this scenario is shown in Figure 6C.

(v) The suggestion that only two catalytic domains unfold in the high-temperature transition of the experimental thermograms is clearly supported by the analysis of the L-Phe effect we give further below which indicates that, at high L-Phe concentrations, only two molecules of L-Phe are released in the high-temperature transition.

*A Simple Model for the Thermal Denaturation of wt-hPAH.* In view of the above, we propose that the thermal denaturation of wt-hPAH, as monitored by DSC, involves three stages:

(i) Unfolding of the four regulatory domains. This process is responsible for the low-temperature transition in the DSC thermograms. We will refer to the protein state with the four regulatory domains unfolded as state R. We note that, according to the experimental calorimetric to van't Hoff enthalpy ratio (Table 1), the N ↔ R transition is not two-state but involves significantly populated intermediate states.

(ii) Unfolding of two catalytic domains. This process is responsible for the high-temperature transition or, at least,

of the part of the high-temperature transition which is amenable to equilibrium thermodynamics analysis (up to about the transition temperature). We will refer to the protein state in which the four regulatory domains and two catalytic domains are unfolded as state C. The experimental calorimetric to van't Hoff enthalpy ratio (Table 1) suggests that the transition R ↔ C is not two-state, but that the two catalytic domains that unfold in this transition might do it in a more or less independent manner.

(iii) Irreversible denaturation of the protein (aggregation and, perhaps, other processes) to yield a final state (F) which is unable to fold back to the native structure. Irreversible denaturation is possibly responsible for the exothermic distortion of the high-temperature transition (reflected in the apparent negative total heat capacity change observed in the experimental thermograms).

Thus, the thermal denaturation of wt-hPAH can be depicted as,[3]

$$\mathrm{N} \xleftrightarrow{\text{four regulatory domains unfold}} \mathrm{R} \xleftrightarrow{\text{two catalytic domains unfold}} \mathrm{C} \xrightarrow{\text{irreversible denaturation}} \mathrm{F} \qquad (7)$$

although we emphasize again that the two equilibrium processes N ↔ R and R ↔ C likely involve significantly populated intermediate states. On the other hand, the interpretation given in eq 7 implies that equilibrium states more unfolded than C are not significantly populated, and, therefore, that equilibrium thermodynamics information about them has been lost [for discussions on the loss equilibrium information caused by irreversible alterations (see refs *31*, *32*, *34*, and *41*)]. Finally, we also note that C → F is just a convenient, phenomenological representation of the irreversible denaturation; actually, the irreversible alteration could occur from other states, even from states that are not significantly populated.

*General Description of the* L*-Phe Effect on the Transition Temperatures for wt-hPAH.* Figure 5 shows the effect of L-Phe concentration on the transition temperatures determined from the fittings described above. Note that both transitions are shifted to higher temperatures upon increasing L-Phe concentration, although the $T_1$ vs. [L-Phe] plot for the low-temperature transition reaches a well-defined plateau for high L-Phe concentrations.

It is important to note here that ligand concentration effects on transition temperatures are not proportional to the fraction of binding sites that are occupied by ligand.[4] In particular, for denaturation processes that involve ligand dissociation, the plot of transition temperature vs ligand concentration does not show a plateau, but the transition temperature keeps increasing with ligand concentration even at concentrations for which binding sites are essentially fully occupied. This important result was demonstrated, for equilibrium transitions, by Julian Sturtevant and co-workers many years ago (*36*, *42*), and it also holds for kinetically controlled transitions, provided that ligand dissociation occurs prior to the rate determining step (*31*). The reason behind this, apparently counterintuitive, behavior has to do with the contribution to the relevant Gibbs energy change that arises from the increase in ligand translational entropy that takes place upon ligand dissociation, a contribution that is proportional to the logarithm of *free* ligand concentration (see, for instance, ref *43*).

In view of the above, the plots of $T_1$ and $T_2$ vs L-Phe concentration of Figure 5 can be qualitatively interpreted as follows: (i) The plot of $T_2$ vs [L-Phe] for the high-temperature transition does not reach a plateau for high L-Phe concentrations, which suggests that L-Phe dissociation occurs upon catalytic domain denaturation. This suggestion is obviously consistent with the presence of L-Phe binding sites in the catalytic domains (which would be destroyed upon denaturation, with the concomitant ligand release). (ii) The high-[L-Phe] plateau in the plot of $T_1$ vs [L-Phe] for the low-temperature transition suggests that L-Phe dissociation does not occur upon regulatory domain denaturation at high [L-Phe]. That is, it suggests that there are no binding sites for L-Phe in the regulatory domain and that the effect of L-Phe concentration on $T_1$ is due to the interaction of the regulatory domain with the catalytic domain (i.e., the regulatory domain detects the binding of ligand to the catalytic domain). This qualitative interpretation is supported by the quantitative analysis we describe below.

*Theoretical Description of Ligand Effects on Transition Temperatures in Terms of Binding Polynomials.* As illustrated by recent work by Hinz and co-workers (*44*, *45*), a great deal of information about ligand-binding energetics can be derived from the analysis of ligand effects on DSC transition temperatures. Here, we will extend this approach in two ways: (i) we will define and use characteristic temperatures, in such a way that the approach can be applied to non-two-state transitions and even to complex, multitransition, calorimetric profiles; (ii) we will describe the ligand effect on the characteristic temperatures in terms of the relevant binding partition functions (binding polynomials), which should allow different binding models to be readily tested and compared. The theoretical relations derived in this

[3] We have made no attempt to justify the differences in stability for the domains in hPAH on the basis of our modeled structure and the known structure-energetics relationships. It must be noted that stability is related to Gibbs energy changes, which are small numbers resulting from the almost complete cancellation of large enthalpic and entropic contributions. Therefore, relative errors in predicted Gibbs energy changes and related parameters are expected to be large. For instance, for a set of model proteins, unfolding enthalpy changes could be predicted from structure to ± 4 kcal/mol (*37*), while the transition temperatures (temperatures at which the unfolding Gibbs energy is zero) at the pH maximal stability were predicted to about ± 10 degrees (*54*).

[4] One of the reviewers of this paper has suggested the possibility that unspecific binding of L-Phe (a substance with hydrophobic character) may contribute significantly to the measured L-Phe effect on transition temperatures. This possibility seems, however, unlikely in this case since: (i) we have used comparatively low L-Phe concentrations; and (ii) unspecific binding of a hydrophobic substance may be expected to occur more extensively to the unfolded state than to the native state; accordingly, increasing the substance concentration will shift the unfolding equilibrium towards the unfolded state with the concomitant decrease in stability and denaturation temperature, an effect which is not observed experimentally (see Figure 6). In connection with the possibility of unspecific L-Phe binding, the same reviewer suggested the convenience of carrying out a control study into the L-Phe effect on the DSC profiles for model proteins that do not have a specific binding site for L-Phe. We have done such a study using ribonuclease A (type XII from Sigma: R-5500), and we have found no detectable L-Phe effect on the DSC profiles within the [L-Phe] range 0−25 mM (the same L-Phe concentration range used in the DSC experiments with hPAH reported in this work). Specifically, the $T_m$ values for ribonuclease A unfolding at pH 6 were 61.6 °C (0 mM L-Phe), 61.8 °C (5 mM L-Phe), 61.9 °C (10 mM L-Phe), and 61.7 °C (25 mM L-Phe).

section will be used in the next one to evaluate and analyze the effect of L-Phe on the DSC thermograms for wt-hPAH. Before beginning the derivations, we wish to emphasize that the L-Phe concentrations employed in this work were, in most experiments, significantly higher than the protein concentration, so that the free ligand concentration can be taken as equal to the total ligand concentration, and we do not need to concern ourselves with the complications that arise when the free ligand concentration changes abruptly during the DSC scan (*44*, *46*−*48*). [In a few experiments, low ligand concentrations (comparable to the protein concentration) were used but, in these cases, the DSC thermograms were essentially identical to those obtained in the absence of L-Phe].

All the equilibrium information regarding the binding of a ligand to a given protein state is contained in the binding partition function or binding polynomial. The binding polynomial is defined as the sum of the statistical weights for all ligation species of the protein, with the statistical weight for a given ligated species ($ML_i$) defined as the ratio of the concentration of that species to that of the unligated species (M). Accordingly, the binding polynomial for a protein with $n$ binding sites for a ligand can be written as (*49*),

$$P = 1 + \sum_{i=1}^{n} \beta_i [L]^i \tag{8}$$

where [L] is the free ligand concentration and $\beta_i$ is the overall Adair constant (*50*) for the equilibrium $M + iL \leftrightarrow ML_i$. We will make use of two important properties of binding polynomials:

(i) The average number of ligand molecules bound per protein molecule can be calculated from the binding polynomial using (see page 67 in ref *49*):

$$\langle i \rangle = \frac{\partial \ln P}{\partial \ln [L]} \tag{9}$$

Therefore, the binding polynomial as a function of free ligand concentration is equivalent to the ligand titration curve ($\langle i \rangle$ vs [L]).

(ii) The binding polynomial is related to the mole fraction of unligated species ($x_M$) through (see page 72 in ref *49*):

$$x_M = 1/P \tag{10}$$

The general expression given above (eq 8) for the binding polynomial in terms of the overall Adair constants is not used often in practice; however, simple and convenient expressions for most binding models can be easily constructed according to rules that have been described in detail in the literature (*49*).

We consider now a DSC transition with clearly defined high-temperature and low-temperature baselines. We will refer to the protein states populated at low and high temperature as A and B states, respectively. We define an equilibrium constant for the conversion $A \leftrightarrow B$ in the absence of ligand as the ratio between the concentrations of the unligated species:

$$K_0 = [B]/[A] \tag{11}$$

In the presence of ligand, there can be ligated species in addition to the unligated ones. Thus, we define an apparent (ligand concentration-dependent) equilibrium constant for the conversion between A and B states in the presence of ligand as:

$$K = [B]_T/[A]_T \tag{12}$$

where $[A]_T$ and $[B]_T$ stand for the total concentrations of A and B states (that is the sum of the concentrations of unligated and ligated species). The two equilibrium constants are related by

$$K_0 = \frac{[B]}{[A]} = \frac{[B]_T x_B}{[A]_T x_A} = K\frac{x_B}{x_A} \tag{13}$$

where $x_A = [A]/[A]_T$ ($x_B = [B]/[B]_T$) is the fraction of the protein present as states of type A (B) which is unligated. These fractions are related to the corresponding binding polynomials through $P_A = 1/x_A$ and $P_B = 1/x_B$ (eq 10). Therefore, eq 13 can be written as

$$K_0 = K\frac{P_A}{P_B} \tag{14}$$

We define now a characteristic temperature for the transition ($T_C$) as the temperature at which the total concentrations of A and B states are equal: $[A]_T = [B]_T$ and, consequently, $K = 1$. Using this definition, eq 14 becomes:

$$\exp\left[-\frac{\Delta H}{R}\left(\frac{1}{T_C} - \frac{1}{T_C^0}\right)\right] = \frac{P_A}{P_B} \tag{15}$$

where $T_C^0$ is the characteristic temperature in the absence of ligand. To arrive to eq 15 from eq 14 we have used that $K = 1$ at the characteristic temperatures and the van't Hoff equation to describe the temperature dependence of $K_0$. We are also assuming that the range of $T_C$ values is narrow so that the enthalpy change for the $A \leftrightarrow B$ transition ($\Delta H$) can be taken as a constant.

Equation 15 gives implicitly the ligand concentration dependence of the transition temperature, provided that model-based expressions for the binding polynomials are supplied, as we will do in the next section.[5] In addition, a

[5] The temperature range spanned by our experimental transition temperature values is comparatively narrow (about 5 degrees for $T_1$ and about 10 degrees for $T_2$), and we have assumed that the unfolding enthalpy change that describes the temperature-dependence of the unfolding equilibrium constant ($K_0$) can be taken as a constant within that narrow range; hence, the left-hand-side term in eq 15 is simply the van't Hoff equation integrated with a constant $\Delta H$ value. Enthalpy changes for ligand-binding processes are usually much smaller than enthalpy changes for unfolding processes; therefore, we also assume in our subsequent analysis (eqs 25−29) that the equilibrium parameters that describe the binding polynomials (right-hand-side of eq 15) can be taken as constants within the narrow range of the transition temperatures. These assumptions, however, are not limitations of the approach and, in fact, temperature dependencies for the unfolding enthalpy and the binding equilibrium parameters could be easily introduced if that is justified by the range and accuracy of the experimental transition temperatures.

useful expression for the slope of a $1/T_C$ vs ln [L] plot can be obtained from eq 15 by solving for $1/T_C$

$$1/T_C = 1/T_C^0 - \frac{R}{\Delta H}\ln\left(\frac{P_A}{P_B}\right) \quad (16)$$

differentiating and using eq 9

$$\frac{d(1/T_C)}{d\ln[L]} = -\frac{R}{\Delta H}\Delta i \quad (17)$$

where $\Delta i$ is number of ligand molecules *released* when A is converted to B:

$$\Delta i = \frac{\partial \ln P_A}{\partial \ln [L]} - \frac{\partial \ln P_B}{\partial \ln [L]} = \langle i\rangle_A - \langle i\rangle_B \quad (18)$$

It is important to note now that the $T_C$ value can be derived from the experimental DSC data without assuming any specific denaturation model; thus, partition functions taking states A and B as reference could be calculated using the Freire-Biltonen double integration procedure (*17*):

$$\ln Q_A = \int_{T_A}^{T} \frac{\langle \Delta H\rangle_A}{RT^2} dT \quad (19)$$

$$\ln Q_B = \int_{T_B}^{T} \frac{\langle \Delta H\rangle_B}{RT^2} dT \quad (20)$$

where $\langle \Delta H\rangle_A$ and $\langle \Delta H\rangle_B$ are the excess enthalpies calculated taking the low-temperature and high-temperature baselines as reference, respectively, and $T_A$ ($T_B$) is a temperature low (high) enough so that all the protein is in states of type A (B). The partition functions $Q_A$ and $Q_B$ are related to the concentrations of the reference states through $Q_A = [P]/[A]_T$ and $Q_B = [P]/[B]_T$, where [P] is the total protein concentration (see ref *17*). Thus, once the temperature dependencies of $Q_A$ and $Q_B$ have been obtained from eqs 19 and 20, the characteristic temperature could be calculated as the temperature at which $Q_A = Q_B$. This involved procedure, however, is not required when the transition is symmetric since, in this case, it is clear (and can be easily demonstrated) that the $Q_A$ vs $T$ and $Q_B$ vs $T$ profiles will cross at the midpoint of the transition. That is, for a symmetric transition the characteristic temperature can be taken as equal to the transition temperature calculated by fitting equations of the type of eq 1. Thus, we may take the $T_1$ and $T_2$ values given in Figure 5 as the characteristic temperatures for the low-temperature and high-temperature transitions (which bypasses the issue of the definition of the baselines for these transitions).

*The Number of Ligand Molecules Released in the Thermally Induced Unfolding Transitions of wt-hPAH.* The inset in Figure 5 shows plots of $1/T_1$ and $1/T_2$ versus ln[L-Phe] for the higher L-Phe concentrations used in this work (2−30 mM). According to eq 17, the numbers of ligand molecules released in the corresponding transitions can be obtained from the slopes of these plots and the experimental $\Delta H$ values of Table 1.

For the low-temperature transition, we obtain $\Delta i = -0.2 \pm 0.2$, that is, a value equal to zero, within the experimental uncertainty, for the number of L-Phe molecules released upon unfolding of the four regulatory domains. This value for $\Delta i$ strongly disfavors the existence of binding sites in the regulatory domains (*10*−*13*, *51*) since these sites would have been destroyed upon regulatory domain unfolding with the concomitant ligand release. This result is also entirely consistent with our assignment of the low-temperature transition to the unfolding of the regulatory domains. Thus, since a maximum of 4−6 mol of L-Phe have been found to bind per tetramer of PAH (*51*−*53*), it seems sound that there are four occupied binding sites at high [L-Phe] in both state N and state R (see eq 7), that is, the four binding sites in the catalytic domains are not destroyed by the unfolding of the regulatory domains.

For the high-temperature transition, we obtain $\Delta i = 1.8 \pm 0.3$, that is, a value close to 2, which strongly supports our assignment of the high-temperature transition to the unfolding of only two catalytic domains. The two remaining L-Phe molecules (bound to the two catalytic domains which remain folded through the high-temperature transition) are presumably released upon irreversible denaturation and, hence, have no effect on $T_2$.

*A Simple Model for the* L*-Phe Effect on the Transition Temperatures of wt-hPAH.* Experimental studies have shown that tetrameric PAH exhibits positive cooperativity for the binding of L-Phe as measured by kinetic (*4*, *8*, *12*) and equilibrium binding analysis (*51*, *52*), with a Hill coefficient of about two. In addition, our modeled structure (Figure 1) indicates that hPAH can be regarded to some extent as a "dimer of dimers". This suggests that a simple, but plausible model for the L-Phe binding to wt-PAH can be constructed by allowing for cooperativity in the binding of L-Phe to a dimer and assuming that the two dimers in tetrameric wt-PAH behave independently of each other with respect to L-Phe binding. In this section, we develop such model and show that it can explain the effect of L-Phe on the transition temperatures $T_1$ and $T_2$. Before proceeding, however, we want to emphasize that we use the word "dimer" in this section to refer to any of the "dimers" into which the structure of wt-hPAH (Figure 1) can be *mentally* split (i.e., we do *not* refer to the truncated form of hPAH that lacks the tetramerization motif and which is actually dimeric in solution).

Specifically, our model is based on the following assumptions:

States N and R (eq 7) can be considered as "dimers of dimers" in which the dimers behave independently of each other with respect to L-Phe binding. This means that the binding polynomial for these states can be written in terms of the binding polynomial for a dimer as (see page 45 in ref *49*)

$$P_{\text{tetramer}} = P_{\text{dimer}}^2 \quad (21)$$

Thus, it is sufficient to describe the binding of L-Phe to a dimer.

Possible cooperativity in the L-Phe binding to a dimer in states N and R (and in the L-Phe binding to state C) can be described phenomenologically in terms of Hill coefficients. This is easily achieved by writing binding polynomials of the form

$$P = [1 + ([L]/C)^{\alpha}]^{n/\alpha} \quad (22)$$

where $n$ is the number binding sites, $\alpha$ is the Hill coefficient, and $C$ is the ligand concentration at which half of the binding sites are occupied by the ligand. Substituting eq 22 into eq 9 the following is easily obtained:

$$\langle i \rangle = n \frac{([L]/C)^{\alpha}}{1 + ([L]/C)^{\alpha}} \tag{23}$$

which can be easily rearranged to yield

$$\ln \frac{\theta}{1-\theta} = \alpha \ln [L] + \alpha \ln K \tag{24}$$

with $\theta = \langle i \rangle / n$ and $K = 1/C$. It is clear, therefore, that the binding polynomial defined in eq 22 is entirely equivalent to the Hill equation (eq 24).

On the basis of eqs 19 and 20, the binding polynomials for the states N, R, and C can be expressed as

$$P_{\mathrm{N}} = \{[1 + ([\mathrm{L-Phe}]/C_{\mathrm{N}})^{\alpha_N}]^{2/\alpha_N}\}^2 \tag{25}$$

$$P_{\mathrm{R}} = \{[1 + ([\mathrm{L-Phe}]/C_{\mathrm{R}})^{\alpha_R}]^{2/\alpha_R}\}^2 \tag{26}$$

$$P_{\mathrm{C}} = [1 + ([\mathrm{L-Phe}]/C_{\mathrm{C}})^{\alpha_C}]^{2/\alpha_C} \tag{27}$$

where $C_{\mathrm{N}}$, $C_{\mathrm{R}}$, and $C_{\mathrm{C}}$ are the concentrations for half-saturation and $\alpha_{\mathrm{N}}$, $\alpha_{\mathrm{R}}$, and $\alpha_{\mathrm{C}}$ are the Hill coefficients for states N, R, and C, respectively.

Applying now eq 16 to the low-temperature and high-temperature transitions we arrive at

$$1/T_1 = 1/T_1^0 - \frac{R}{\Delta H_1} \ln \left( \frac{P_{\mathrm{N}}}{P_{\mathrm{R}}} \right) \tag{28}$$

$$1/T_2 = 1/T_2^0 - \frac{R}{\Delta H_2} \ln \left( \frac{P_{\mathrm{R}}}{P_{\mathrm{C}}} \right) \tag{29}$$

Equation 28, together with eqs 25 and 26, provides the theoretical dependence of $T_1$ with L-Phe concentration. Likewise, eq 29, together with eqs 26 and 27, provides the theoretical dependence of $T_2$ with [L-Phe]. Since the binding polynomial for state R (eq 26) is involved in both theoretical dependencies, we have carried a simultaneous fitting of these dependencies to the $T_1$ vs [L-Phe] and $T_2$ vs L-Phe profiles. The values of $\Delta H_1$ and $\Delta H_2$ were fixed in the experimental values given in Table 1, and $T_1^0$, $T_2^0$, $C_{\mathrm{N}}$, $C_{\mathrm{R}}$, $C_{\mathrm{C}}$, $\alpha_{\mathrm{N}}$, $\alpha_{\mathrm{R}}$, and $\alpha_{\mathrm{C}}$ were fitting parameters, although the values of the Hill coefficients were restricted to the 1−2 range (note that, in our model, the value of the Hill coefficient cannot be larger than the number of sites in a dimer). The fitting was excellent (see Figure 5), and the values derived for the fitting parameters, together with the corresponding standard errors, are collected in Table 3. The value found for the Hill coefficient in the state N has a comparatively large associated standard error ($\alpha_{\mathrm{N}} = 2 \pm 0.9$), but it appears to be consistent with the Hill coefficient obtained in previous binding studies (*51*, *52*). On the other hand, the value found for the Hill coefficient in state R ($\alpha_{\mathrm{R}} = 1 \pm 0.17$) suggests that cooperativity in the binding of L-Phe to the catalytic domains is lost upon regulatory domain unfolding. The interaction between the regulatory and catalytic domains is also reflected in the value for the half-saturation concentration, which is significantly increased upon regulatory domain unfolding (see the values of $C_{\mathrm{N}}$ and $C_{\mathrm{R}}$ in Table 3).

Table 3: Values of the L-Phe Concentrations Corresponding to Half Saturation (C), Hill Coefficients ($\alpha$) and Transition Temperatures ($T_1^0$) in the Absence of L-Phe, Derived from the Fitting of the Dependencies Given by Eqs 25−29 to the Experimental $T_1$ and $T_2$ versus [L-Phe] Profiles[a]

| | | |
|---|---|---|
| $C_{\mathrm{N}} =$ 0.072 ± 0.017 mM | $C_{\mathrm{R}} =$ 0.268 ± 0.066 mM | $C_{\mathrm{C}} =$ 2.45 ± 1.10 mM |
| $\alpha_{\mathrm{N}} = 2 \pm 0.94$ | $\alpha_{\mathrm{R}} = 1 \pm 0.18$ | $\alpha_{\mathrm{C}} = 2 \pm 3.0$ |
| $T_1^0 = 319.5 \pm 0.3$ K | $T_2^0 = 328.5 \pm 0.3$ K | |

[a] See text.

## CONCLUDING REMARKS

We have shown that the two transitions seen in the DSC thermograms for the thermal denaturation of tetrameric wt-hPAH can be assigned to the unfolding of the four regulatory domains (low-temperature transition) and two catalytic domains (high-temperature transition), while irreversible denaturation is likely responsible for the exothermic distortion of the high-temperature side of the high-temperature transition.

We have developed an equilibrium thermodynamics approach to the analysis of ligand effects on DSC transitions, which is based upon the general binding polynomial formalism and is not restricted to two-state transitions. This approach may allow different binding models to be tested and compared, since binding polynomials for most binding models can be easily written following rules which have been described in detail in the literature (see, for instance, ref *49*). In this work, we have derived and used expressions for the binding polynomials that are consistent with the phenomenological description of cooperativity in ligand binding in terms of Hill coefficients.

Our analysis of the L-Phe effect on the DSC transition temperatures for wt-hPAH supports the following:

No binding sites for L-Phe are present in the regulatory domain. This disfavors interpretations of the cooperative activation of PAH as a result of the binding of L-Phe to a putative allosteric/regulatory site, which is different from the catalytic sites, and support our proposal (*14*, *15*) that the activation of PAH by L-Phe is the result of its homotropic cooperative binding at the active sites.

There is interaction between the regulatory and the catalytic domains. This is reflected in the results of our model-based fittings to the transition temperature vs [L-Phe] profiles, which suggest that, upon regulatory domains unfolding, the cooperativity in the binding of L-Phe to the catalytic domains is lost and the L-Phe concentration for half-saturation is significantly increased.

Finally, we want to propose that, in addition to the interactions of the catalytic and regulatory domains, those of the tetramerization motif are also involved in cooperativity. Thus, as seen in our modeled structure (Figure 1), residues from a loop (68−75) in the regulatory domain establish contacts with the start of the helical tetramerization motif. Moreover, each of these motifs establishes contacts with the tetramerization helices from two other subunits suggesting that changes in the interactions between the helix bundle and the rest of the domains might be the way in which the cooperative conformational changes induced by L-Phe is

transmitted in tetrameric wt-hPAH. In fact, the binding of L-Phe to a truncated hPAH form lacking the tetramerization motif [dimeric hPAH(Ser2−Arg428)] was found to be noncooperative (*4*), and our preliminary DSC studies indicate that, in contrast to what is seen in wt-hPAH, L-Phe binding to the catalytic domains in this truncated form does *not* affect the unfolding transition for the regulatory domains (work in progress).

## ACKNOWLEDGMENT

We are very grateful to Per M. Knappskog for preparation of bacterial strains expressing human phenylalanine hydroxylase.

## REFERENCES

1. Kappock, T. J., and Caradonna, J. P. (1996) *Chem. Rev. 96*, 2659−2756.
2. Flatmark, T., and Stevens, R. C. (1999) *Chem. Rev. 99*, 2137−2160.
3. Dickson, P. W., Jennings, I. G., and Cotton, R. G. (1994) *J. Biol. Chem. 269*, 20369−20375.
4. Knappskog, P. M., Flatmark, T., Aarden, J. M., Haavik, J., and Martínez, A. (1996) *Eur. J. Biochem. 242*, 813−821.
5. Erlandsen, H., Fusetti, F., Martínez, A., Hough, E., Flatmark, T., and Stevens, R. C. (1997) *Nat. Struct. Biol. 4*, 995−1000.
6. Fusetti, F., Erlandsen, H., Flatmark, T., and Stevens, R. C. (1998) *J. Biol. Chem. 273*, 16962−16967.
7. Kobe, B., Jennings, I. G., House, C. M., Michell, B. J., Goodwill, K. E., Santarsiero, B. D., Stevens, R. C., Cotton, R. G., and Kemp, B. E. (1999) *Nat. Struct. Biol. 6*, 442−448.
8. Kaufman, S. (1993) *Adv. Enzymol. Relat. Areas Mol. Biol. 67*, 77−264.
9. Kaufman, S. (1987) *Enzyme 38*, 286−295.
10. Tourian, A. (1971) *Biochim. Biophys. Acta 242*, 345−354.
11. Shiman, R., Xia, T., Hill, M. A., and Gray, D. W. (1994) *J. Biol. Chem. 269*, 24647−24656.
12. Parniak, M. A. (1987) in *Unconjugated Pterins and Related Biogenic Amines* (Curtius, H.-C., and Blau, N., Eds.) pp 327−337, Walter de Gruyter & Co., Berlin.
13. Gjetting, T., Petersen, M., Guldberg, P., and Guttler, F. (2001) *Am. J. Hum. Genet. 68*, 1353−1360.
14. Martínez, A., Haavik, J., and Flatmark, T. (1990) *Eur. J. Biochem. 193*, 211−219.
15. Martínez, A., Olafsdottir, S., and Flatmark, T. (1993) *Eur. J. Biochem. 211*, 259−266.
16. Erlandsen, H., and Stevens, R. C. (1999) *Mol. Genet. Metab. 68*, 103−125.
17. Freire, E., and Biltonen, R. L. (1978) *Biopolymers 17*, 463−479.
18. Brandts, J. F., Hu, C. Q., and Lin, L.-N. (1989) *Biochemistry 28*, 8588−8596.
19. Ramsay, G., and Freire, E. (1990) *Biochemistry 29*, 8677−8683.
20. Freire, E., Murphy, K. P., Sanchez-Ruiz, J. M., Galisteo, M. L., and Privalov, P. L. (1992) *Biochemistry*, 250−256.
21. Martínez, A., Knappskog, P. M., Olafsdottir, S., Døskeland, A. P., Eiken, H. G., Svebak, R. M., Bozzini, M., Apold, J., and Flatmark, T. (1995) *Biochem. J. 306*, 589−597.
22. Chehin, R., Thorolfsson, M., Knappskog, P. M., Martínez, A., Flatmark, T., Arrondo, J. L., and Muga, A. (1998) *FEBS Lett. 422*, 225−230.
23. Ibarra-Molero, B., Makhatadze, G. I., and Sanchez-Ruiz, J. M. (1999) *Biochim. Biophys. Acta 1429*, 384−390.
24. Shrake, A., and Rupley, J. A. (1973) *J. Mol. Biol. 79*, 351−371.
25. Chothia, C. (1976) *J. Mol. Biol. 105*, 1−12.
26. MacColl, R., Malak, H., Gryczynski, I., Eisele, L. E., Mizejewski, G. J., Franklin, E., Sheikh, H., Montellese, D., Hopkins, S., and MacColl, L. C. (1998) *Biochemistry 37*, 417−423.
27. Urban, C., and Schurtenberger, P. (1998) *J. Colloid Interface Sci. 207*, 150−158.
28. Ferrin, T. E., Hunag, C. C., Jarvis, L. E., and Langridge, R. (1988) *J. Mol. Graphics 6*, 13−27.
29. Ledley, F. D., Grenett, H. E., and Woo, S. L. (1987) *J. Biol. Chem. 262*, 2228−2233.
30. Kleppe, R., Uhlemann, K., Knappskog, P. M., and Haavik, J. (1999) *J. Biol. Chem. 274*, 33251−33258.
31. Sanchez-Ruiz, J. M. (1992) *Biophys. J. 61*, 921−935.
32. Plaza del Pino, I. M., Ibarra-Molero, B., and Sanchez-Ruiz, J. M. (2000) *Proteins 40*, 58−70.
33. Vogl, T., Jattzke, C., Hinz, H.-J., Benz, J., and Huber, R. (1997) *Biochemistry 36*, 1657−1668.
34. Sanchez-Ruiz, J. M. (1995) in *Subcellular Biochemistry, Volume 24. Proteins: Structure, Function and Engineering* (Biswas, B. B., and Roy, S., Eds.) pp 133−176, Plenum, New York.
35. Takahashi, K., and Sturtevant, J. M. (1981) *Biochemistry 20*, 6185−6190.
36. Manly, S. P., Mathews, K. S., and Sturtevant, J. M. (1985) *Biochemistry 24*, 3842−3846.
37. Hilser, V. J., Gómez, J., and Freire, E. (1996) *Proteins 26*, 123−133.
38. Luque, I., Gómez, J., and Freire, E. (1998) *Proteins 30*, 74−85.
39. Levitt, M. (1974) *J. Mol. Biol. 82*, 393−420.
40. Izatt, R., and Christensen, J. (1976) (Fasman, G., Ed.) pp 153−269, CRC press, Cleveland, Ohio.
41. Freire, E., van Osdol, W. W., Mayorga, O. L., and Sanchez-Ruiz, J. M. (1990) *Annu. Rev. Biophys. Biophys. Chem. 19*, 159−188.
42. Fukada, H., Sturtevant, J. M., and Quiocho, F. (1983) *J. Biol. Chem. 258*, 13193−13198.
43. Chan, H. S., and Dill, K. A. (1997) *Annu. Rev. Biophys. Biomolec. Struct. 26*, 425−459.
44. Rösgen, J., and Hinz, H. J. (2001) *J. Mol. Biol. 306*, 809−824.
45. Rosengarth, A., Rösgen, J., Hinz, H. J., and Gerke, V. (2001) *J. Mol. Biol. 306*, 825−835.
46. Robert, C. H., Gill, S. J., and Wyman, J. (1988) *Biochemistry 27*, 6829−6835.
47. Brandts, J. F., and Lin, L. N. (1990) *Biochemistry 29*, 6927−6940.
48. Shrake, A., and Ross, P. D. (1990) *J. Biol. Chem. 265*, 5055−5059.
49. Wyman, J., and Gill, S. J. (1990) *Binding and Linkage. Functional Chemistry of Biological Macromolecules*, University Science Books, Mill Valley, California.
50. Adair, G. S. (1925) *J. Biol. Chem. 63*, 529−545.
51. Phillips, R. S., Parniak, M. A., and Kaufman, S. (1984) *J. Biol. Chem. 259*, 271−277.
52. Parniak, M. A., and Kaufman, S. (1981) *J. Biol. Chem. 256*, 6876−6882.
53. Shiman, R. (1980) *J. Biol. Chem. 255*, 10029−10032.
54. Hilser, V. J., Townsend, B. D., and Freire, E. (1997) *Biophys. Chem. 64*, 69−79.

BI0160720